An IoT Solution for Online Monitoring of Anesthetics in Human Serum Based on an Integrated Fluidic Bioelectronic System

Francesca Stradolini, Abuduwaili Tuoheti, Tugba Kilic, Sofia Lydia Ntella, Nadia Tamburrano, Zijian Huang, Giovanni De Micheli, Danilo Demarchi, and Sandro Carrara

***Abstract*—In this paper, we present the design, the implementation and the validation of a novel *Internet of Things* (IoT) drug monitoring system for the online continuous and simultaneous detection of two main anesthetics, e.g., propofol and paracetamol, in undiluted human serum. The described full system consists of a custom-built electronic *Raspberry Pi* (RPi) based *Printed Circuit Board* (PCB) that drives and reads out the signal from an electrochemical sensing platform integrated into a fluidic system. Thanks to the *Polydimethylsiloxane* (PDMS) fluidic device, the analyzed sample is automatically fluxed on the sensing site. The IoT network is supported by a Cloud system, which allows the doctor to control and share all the patient's data through a dedicated Android application and a smart watch. The validation closes with the first ever demonstration that our system successfully works for the simultaneous monitoring of propofol and paracetamol in undiluted human serum by measuring the concentration trends of these two drugs in fluxing conditions over time.**

***Index Terms*—Anesthesia, electrochemical sensors, fluidics, human serum detection, pencil graphite electrodes, Raspberry-Pi, therapeutic drug monitoring.**

I. Introduction

GENERAL anesthesia is a drug-induced, reversible condition in which the patient is unconscious and unresponsive to painful surgical stimuli [1], [2]. This sedation status is achieved by intravenous (i.v.) administration of a cocktail of drugs; such as muscle relaxant, hypnotic, and analgesic [3]. The correct balance of these i.v. medications is crucial to ensure a rapid onset and an accurate *Depth of Anesthesia* (DOA) during the induction phase, as well as to guarantee a pleasant and short recovery time after surgery [4].

Propofol is a widely used anesthetic thanks to its many pharmacological properties such as rapid distribution, short action and reduced side effects in post-operative recovery [5]. However, its administration causes pain or discomfort in 28%–90% of patients [6]. This is known as *Pain On Propofol Injection* (POPI) and it is still among the most critical problems in the anesthesia current practices [7]. To reduce POPI effects, other compounds, e.g., paracetamol, are usually administered in combination with propofol [6] to exploit their antipyretic and analgesic effects [8]. Nowadays, common practice for the intravenous administration of these anesthetic compounds is to use *Target Controlled Infusion* (TCI) pumps [9]. TCI systems rely on advanced *PharmacoKinetic* (PK) models that quantitatively predict the plasma concentration of the drug and adjust the delivery rate accordingly [10]. However, due to inter- and intra-patients' variability, these models can be affected by up to 30%−50% of inaccuracy [11] and they cannot predict the direct relation between drug kinetics and its clinical effects [12]. To improve the accuracy of the drug administration, the anesthesiologist constantly monitors the *ElectroEncephaloGram* (EEG) signal and the *Bispectral Index* (BIS), which can be related with the DOA. However, since both these two clinical parameters are evaluated in an indirect manner, therefore, they don't provide information with respect to actual drug concentration and moreover they might be affected by noise and artifacts [13]–[15]. To overcome these limitations, *Therapeutic Drug Monitoring* (TDM) systems measuring the actual drug concentration in patient's plasma are in huge demand since they would provide TCI pumps with the actual drug concentration to perform perfusion. Thanks to those systems, the anesthetic infusion rate and dosage would be dynamically adjusted to meet personal requirements. Electrochemical sensors are considered as ideal devices for the realization of such monitoring systems due to their high sensitivity, specificity, simplicity that allow an accurate, rapid and quantitative detection of drugs [16]. A typical electrochemical measurement system requires: (i) a three-electrode sensing cell (*Working, Reference* and *Counter Electrodes*, WE - RE - CE, respectively) in direct contact with the analyte solution, and (ii) a potentiostat that drives the electrochemical measurements and reads out the signal [17].

Manuscript received February 14, 2018; revised May 7, 2018; accepted July 6, 2018. Date of publication July 31, 2018; date of current version October 19, 2018. This work was supported in part by the CoMofA project under Grant 325230-157139 and in part by the Swiss National Science Foundation. This paper was recommended by Associate Editor F. Corinto. *(Corresponding author: Francesca Stradolini.)*

F. Stradolini, T. Kilic, S. L. Ntella, Z. Huang, G. De Micheli, and S. Carrara are with the Integrated Systems Laboratory, EPFL, 1015 Lausanne, Switzerland (e-mail: francesca.stradolini@epfl.ch; tugba.kilic@epfl.ch; dellalydia@gmail.com; zijian.huang@epfl.ch; giovanni.demicheli@epfl.ch; sandro.carrara@epfl.ch).

A. Tuoheti and N. Tamburrano are with the Integrated Systems Laboratory, EPFL, 1015 Lausanne, Switzerland, and also with the Department of Electronics and Telecommunications, Politecnico di Torino, 10129 Torino, Italy (e-mail: abuduwaili.tuoheti@studenti.polito.it; nadia.tamburrano@epfl.ch).

D. Demarchi is with the Department of Electronics and Telecommunications, Politecnico di Torino, 10129 Torino, Italy (e-mail: danilo.demarchi@polito.it).

Color versions of one or more of the figures in this paper are available online at http://ieeexplore.ieee.org.

Digital Object Identifier 10.1109/TBCAS.2018.2855048

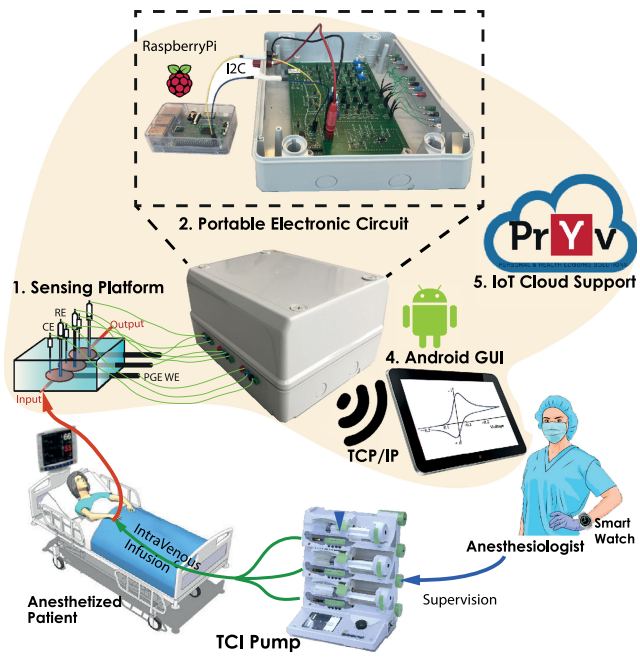

Fig. 1. Sketch of the IoT system (orange part) for the on-line continuous and simultaneous detection of anesthetics proposed to be a part of real hospital settings.

Therefore, the present work focuses on the design, implementation and validation of a novel IoT drug monitoring system for the on-line continuous and simultaneous detection of two main anesthetics, the propofol and the paracetamol, in undiluted human serum. By applying IoT solutions to medical systems (mIoT), it is possible to realize powerful tools able to provide rapid and precise information on patients' health status to the medical staff at any time and from any hospital area [18]. Therefore, an improved and constant patient care and monitoring is achieved [19]. The sketch of our system is represented in Fig. 1. Up to now, there has not been any complete system with a sensing module integrated with electronic circuit board that targets anesthesia monitoring for multiple sensing being proposed. Although Myers *et al.* proposed a feedback controlled infusion of organic-based drugs towards safer anesthesia monitoring [20], the simultaneous detection of different drugs, development of custom-built board and IoT support were not provided. In addition to that, other groups developed various strategies for monitoring anesthetics via electrochemical methods and liquid chromatography without integration to an electronic board. The novelty of our system compared to the recent literature relies on the fact that a full system comprising: (i) a low-noise, custom-built electronic potentiostatic PCB driven by a RPi, (ii) the electrochemical sensing platform integrated into (iii) a fluidic system which directs the sample on the sensing site and (iv) an IoT network including a Cloud system that allows the doctor to control and share all the patient's data through a dedicated Android application has been developed in the current work.

The comparison with other systems published until now for the detection of anesthetics or other metabolites is not so straightforward, since these works focus on different applications [21], or present other techniques for propofol detection that are costly and bulky [22], [23] and even the already presented electrochemical sensors for propofol sensing do not provide yet a fully mature IoT monitoring system [24]–[26].

In the following Section II the architecture of our system will be described in details of each of its main parts. Then, the validation of the system and the proprofol and paracetamol simultaneous monitoring in undiluted human serum will be presented in Section III. Finally, Section VI concludes the work.

II. The System Architecture

In this section we present an overview of the PoC system for propofol and paracetamol anesthetics monitoring. In the first subsection we show the design of the control and readout circuitries driven by the RPi, then the following subsection introduces the sensing platform for anesthetic detection completed by pH and T sensing. Third subsection describes the fluidic platform, and finally the last subsection contains the details on the cloud-based Android network.

A. The Electronic Front-end and the 4th-order Filter Hardware Implementation

1) Hardware Analysis: We have redesigned the front-end hardware of our previous implementation [27] by improving its performances with the aim of providing a robust system for human serum detection. In particular, we have re-implemented the analog read-out by introducing a 4th-order filtering block as second amplification stage in cascade with respect to the *Trans-Impedance Amplifier* (TIA) stage. Therefore, the hardware architecture of the complete system, shown in Figure 2, consists of a RPi as central control unit, which embeds a *Graphical User Interface* (GUI) for setting up and configuring the front-end for the specific electrochemical experiments to run. The RPi controls (master) the *ATxmega32E5* micro-controller (slave) on the custom-built PCB *via* I^2C port. The *ATxmega32E5* micro-controller was chosen for its easy-to-use resources and hardware, such as internal counters, analog input channels, *Serial Peripheral Interface* SPI ports, I^2C ports that are enough for the current application. The wireless communication between the RPi and the Android-based cloud network exploits the *Transmission Control Protocol/Internet Protocol* (TCP/IP). Communication bandwidth was evaluated to be 3.25 Mbit/s in download and 10.13 Mbit/s in upload.

Up to now, designed electronic boards for the purpose of electrochemical measurements either target only certain metabolites detection such as neurotransmitters or capable of doing potentiostatic measurements. None of the proposed system [28]–[31], provided the complete set of voltammetric techniques with the possibility to perform different techniques simultaneously through independent channels. By our design simultaneous detection of multiple drugs (up to three) *via* DPV, CV and CA as well as pH and temperature measurements can be achieved in a single platform. This platform, of which dimensions are 12 cm $\times$ 14 cm and it is made up of only two layers, relies on the *ATxmega32E5* micro-controller, which simultaneously drives 3 independent *actuation* and *sensing* blocks for interfacing with three separated electrochemical cells. Each *actuation* block includes: a 10-bit *MCP4911 Digital to Analog Converter*

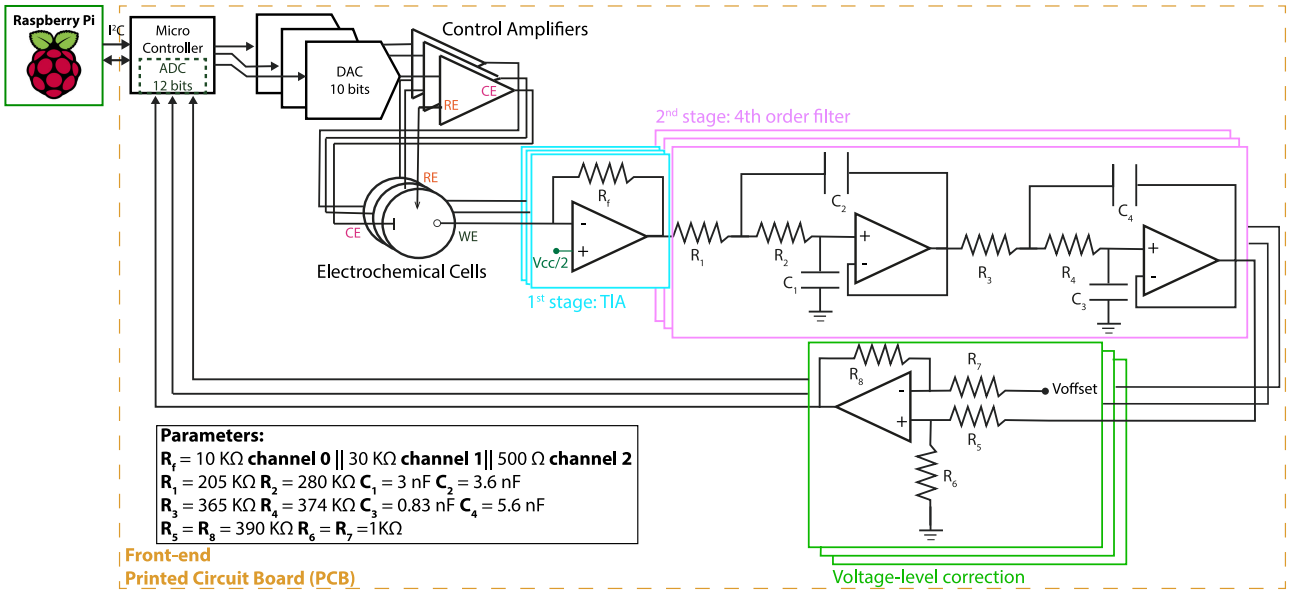

Fig. 2. Schematic of the portable electronic platform consisting of a RPi driving a custom-built PCB circuit through I²C serial communication. Inset shows the parameters chosen for the circuit components.

(DAC) from Microchip and an operational amplifier (Op-Amp) *MAX4475ASA+* from Maxim Integrated. Each *sensing* block consists of a 3-stage signal processing: i) current-to-voltage conversion, ii) filtering, iii) voltage-level correction.

1) *Current-to-voltage conversion*
This stage (blue square in Figure 2), consisting in a TIA, converts the current from the WE into a voltage signal. To minimize the noise, the MAX4475ASA+ Op-Amp was chosen for its low noise, low distortion and low input-bias current characteristics [32]. Besides that, a low noise feedback resistor with 0.1% tolerance is used.

2) *Filtering*
This stage (pink square in Figure 2) implements a 4th order Butterworth low-pass filter with unity-gain Sallen-Key topology. The Butterworth low-pass filter is selected as it gives the maximum passband flatness for the incoming signal [33] and it offers a higher roll off to the input signals beyond the cut-off frequency compared to lower order [34]. The smallest pulse period during measurement is 68 ms, as indicated in Table II, which corresponds to a frequency of around 15 Hz. Therefore, the cut-off frequency f_c of the filter was set at 200 Hz. We have used MAX4477ASA+ Op-Amp since it has a gain bandwidth product of 10 MHz which is much higher than the filter f_c. Since the Op-Amp gain starts to fall at 1 KHz, we have unity gain at 200 Hz. Therefore, the finite gain bandwidth product has negligible effects on the characteristics of the filter. In addition, the output impedance of MAX4477ASA+ is ∼0.02 Ohm; then, respect to the resistors connected in series to its output, we can neglect its effect.
Since the 4th order Butterworth filter is designed as 2-stage cascaded Sallen-Key 2nd order filters, we have derived the overall transfer function starting from the one of the second-order Sallen-Key filter:

$$H_{SK}(s) = \frac{V_{\text{out}}(s)}{V_{\text{in}}(s)} = \frac{1}{[1+\omega_c C_1(R_1+R_2)s+\omega_c^2 C_1 C_2 R_1 R_2 s^2]} \quad (1)$$

Hence, the overall final transfer function is given by:

$$H_{BW}(s) = \frac{1}{[1+\omega_c C_1(R_1+R_2)s+\omega_c^2 C_1 C_2 R_1 R_2 s^2]} \times \frac{1}{[1+\omega_c C_3(R_3+R_4)s+\omega_c^2 C_3 C_4 R_3 R_4 s^2]} \quad (2)$$

Where $\omega_c = 2\pi f_c$ and f_c is the cut-off frequency of the filter. By comparing the denominator with the 4th order normalized Butterworth polynomials:

$$B_4(s) = \left(s^2 + 1.8478s + 1\right)\left(s^2 + 0.7654s + 1\right) \quad (3)$$

the values of R_1, R_2, R_3, R_4 were decided after choosing appropriate values for C_1, C_2, C_3 and C_4. The chosen parameters are reported in Figure 2.
To evaluate the overall noise of the circuit, we considered the equivalent noise bandwidth that can be calculated from:

$$\omega_{enbw} = \int_{-\infty}^{\infty} \left|\frac{H(j\omega)}{H_{\max}}\right|^2 d\omega \quad (4)$$

Where the $H_{\max}$ is the maximum value of the transfer function $H(s)$ or $H(j\omega)$. Knowing the transfer function $H(s)$ and the cut-off frequency ($f_c = 200$ Hz), the calculated equivalent noise bandwidth is equal to 35.37 rad/s,

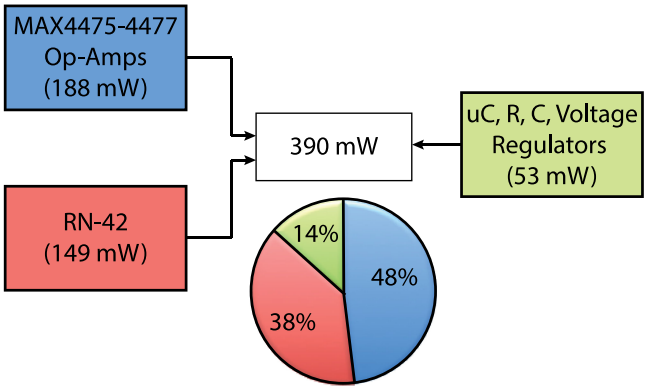

Fig. 3. Schematic representation of the front-end power consumption analysis with percentage estimation.

which corresponds to 222 Hz in frequency. So, the total *root mean square* (rms) noise over the bandwidth is 3.5641 μV and the input referred current noise at 1 Hz frequency is 19.497588 pA.

3) *Voltage-level correction*
The voltage signals at the output of the sensing blocks are measured by the 12-bit ADC inside the Micro-controller, furthermore, the reference voltage of the ADC is configured as 2 V. So, the voltage-level correction stage (green box in Figure 2) is added after the filtering stage in order to guarantee that the voltage signal is in the input range of ADC.

2) Power Consumption Analysis: The main contribution for the power consumption of the electronic board comes from two sets of components: the MAX4475 and MAX4477 Op-Amps and the Classical Bluetooth Module RN-42. The *ATxmega32E5* micro-controller and the rest of the components consume far less then these mentioned ones. From the data-sheet of MAX4475 and MAX4477, the typical power consumption with 5V power supply is around 12.5 mW, which can reach a maximum value of 22 mW. Since within the PCB circuit there are 15 Op-Amps in total, the final contribution is around 188 mW. While the typical power consumption of the RN42 is around 149 mW. Therefore, the two types of components contribute to a typical 337 mW. Finally, we have measured the power consumption of the entire electronic board at 5V power supply during the simultaneous measurements on the three channels. The total current consumption was measured to be 78 mA; hence, the power consumption was calculated to be 390 mW. Fig. 3 schematically represents the contributions of the different front-end parts in the power consumption analysis. Since the measurements are taken periodically, we shut down both the MAX4475 and MAX4477 Op-Amps and RN-42 when any measurement is taking place.

B. The Electrochemical Sensing Platform

1) Drug Sensing: Main challenge dealing with electrochemical detection of propofol is related to the fouling phenomenon triggered by its oxidation. Propofol is a phenolic compound and its oxidation results in free radicals. Hence, after prolonged measurements, free radicals cause electro-polymerization leading to the formation of a passivation fouling layer on the sensor surface, which decreases the sensitivity over time [35]. In our previous studies, we have demonstrated that *Pencil Graphite Electrode* (PGE) provides a suitable substrate for propofol detection and we have identified the lead composition corresponding to the letter *3H* in the *European Letter Scale* (58% graphite, 36% clay and 5% wax) as the optimum in terms of resistance against fouling and long-term stability [36]. In our work [37], we have also demonstrated with an interference study that, dual detection of propofol and paracetamol can be achieved successfully by PGE. Consequently, our fabricated circuit is designed to work in combination with an electrochemical cell consisting of a *3H* PGE electrode as WE, an Ag/AgCl as RE and a Pt wire as CE.

TABLE I
FLUID PARAMETERS SET FOR COMSOL SIMULATION

	serum solution
density (g/mL)	1.0242 [41]
viscosity (mPa·s)	1.27 [42]

2) pH and Temperature: Since temperature and pH affect the reactivity of chemical species, and hence the calibration results due to peak potential shift, electrochemical sensors designed for drug monitoring needs to be calibrated for various temperature and pH values encountered over time. The design, fabrication and test of this part of the system was already presented in [38] which is driven by the RPi, core of our architecture. We have shown in our previous work [38] that, calibration curves change over a range of temperature and pH values for propofol and any concentration evaluation should be done according to the corresponding calibration curves. Briefly, the temperature is measured with the waterproof DS18B20 direct-to-digital temperature sensor by *Maxim IC*, while the pH is measured with the glass potentiometric *EXTECH* electrode, both connected on the board. The temperature measurements are transferred to the RPi through 1-wire communication, while the differential potential in mV coming from the glass electrode is converted to digital and transferred to the the same platform through *Serial Peripheral Interface* (SPI) where it is translated into a pH value according to the Nernst equation [39].

C. The Fluidic Device

The fluidic device has been designed to guide the sample on the sensing platform and to optimize the mixing properties of the electrochemical chamber. Three different geometries have been tested before the fabrication by running *Laminar Flow Single Phase* in-built simulations of Comsol Multiphysics software. In this step, the laminar flow was ensured by adopting an appropriate Reynold value and by evaluating the inlet flow velocity μ by the flow rate $Q = 10.4$ μl/s ad $\mu = Q/A = 0.053$ m/s, where A is the cross section area of the inlet (radius $= 0.25$ mm). Pressure at the inlet/outlet was set to zero and suppress the back flow at the outlet. The domain equation in the Comsol model is incompressible Navier-Stokes equation, which is used for the main chamber to describe the fluid property [40]. The parameter

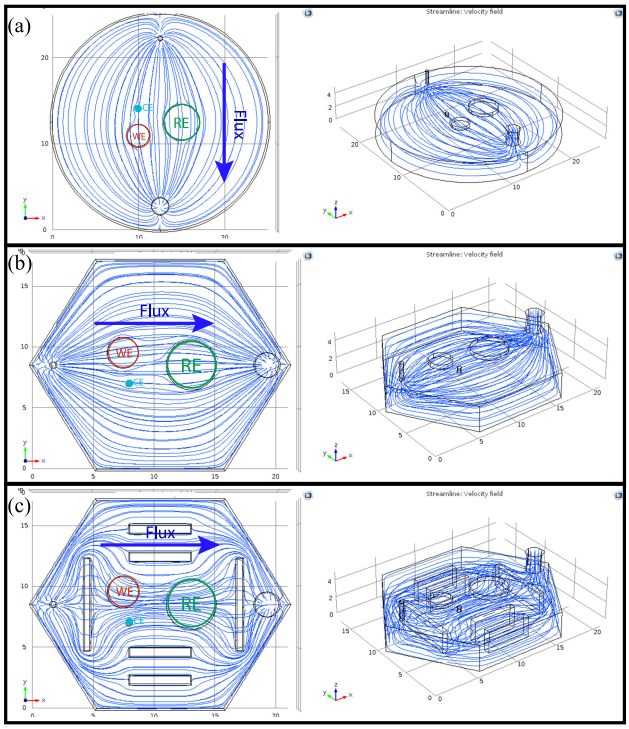

Fig. 4. Comsol simulations results for different geometries of fluidic chambers: (a) circular, (b) hexagonal, and (c) hexagonal with internal walls.

values for the fluid were set as in the Table I to simulate serum solution flow.

Fig. 4 summarizes the simulation output obtained from the three different geometries tested for the fluidic chamber: (i) round, (ii) hexagonal and (iii) hexagonal with internal walls. The passive sensing platform consists of a PGE WE (2.5 mm ⌀) an Ag/AgCl RE (4 mm ⌀) and Pt-wire CE (0.5 mm ⌀) that corresponds to the three holes on the top of the chamber. As we can deduce form the simulation results in Fig. 4, the internal soft-walls, which act as obstacles for the fluid flow, facilitate the internal mixing by causing turbulences. Hence, the fluidic chamber was realized in PDMS following this optimized geometry.

D. IoT Architecture: An Android Application with Cloud Support

To facilitate the portability of the system, we have introduced the possibility for the anesthesiologist to continuously keep under control the patients through an Android application and a smart-watch [43]. This application not only offers a fast (approximately <2 s) and user-friendly visualization of the data received *via* WiFi from the sensing platform, but it also allows the medical doctor to share and store the patient's data on a cloud solution (with latency time under 100 ms for an event creation call on Cloud, as comparable to a standard HTTP request). In this way, the data are accessible from everywhere and at any time through a web application, hence enabling teleconsulting. Thanks to this network, the doctor is allowed to freely move and perform other tasks without losing the control on the anesthetized patients. Indeed, if a connected patient registers an out-of-safe-range parameter, then the tablet/smart-phone where the Andorid app is running starts to tremble and, furthermore, an alert (approximately <3 s) is sent from the app to the doctor's smart-watch to notify the emergency. The alert on the smart-watch consists on a strong vibration and a pop-up including the name of the in-danger patient and the information about the critical parameter recorded. Both the Android and the web applications, shown in Fig. 5, handle a secure management of the patients' data, by guaranteeing access only to authorized doctors and the *HyperText Transfer Protocol Secure* (HTTPS) ensures a secure data transmission over the Internet.

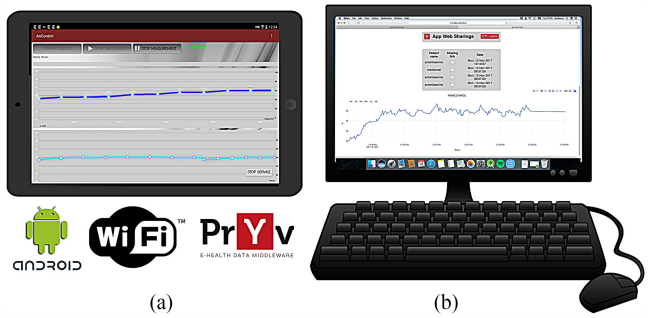

Fig. 5. Graphical user interface screen-shots for the IoT network: (a) Android interface running on a tablet or smartphone of the anesthesiologist in charge and (b) web application to remotely access patients' data from anywhere and at any time.

TABLE II
ELECTROCHEMICAL MEASUREMENT PARAMETERS

DPV Measurements APAP		
Start-V (mV)	End-V (mV)	V-Step (mV)
-100	1100	5
Pulse-Width (ms)	Pulse-Ampl. (mV)	Pulse Period (ms)
50	90	68
DPV Measurements Propofol		
Start-V (mV)	End-V (mV)	V-Step (mV)
0	1100	5
Pulse-Width (ms)	Pulse-Ampl. (mV)	Pulse Period (ms)
75	90	102
CA Measurements: APAP and Propofol		
APAP Applied Voltage (mV)	Propfol Applied Voltage (mV)	
900	1000	

III. RESULTS AND DISCUSSION

A. Materials and Methods

1) Hardware Setup: The driving core of the hardware architecture is the RPi 3 Model B V-1.2, which is an embedded Linux computer with Raspbian OS installed. A dedicated GUI in the RPi has been realized in Qt Creator 3.2 software with Qt 5.3 libraries. The RPi controls, powers (5V) and sets the PCB's parameters according to the desired measurement to be performed. Both *ChronoAmperometry* (CA) and *Differential Pulse Voltammetry* (DPV) measurements have been used to validate the system for propofol and APAP detection and the corresponding parameters are summarized in Table II. Whenever a new data is read from the sensing platform, it is send by RPi via Wi-Fi to the Android application running on the anesthesiologist's tablet or smart-phone.

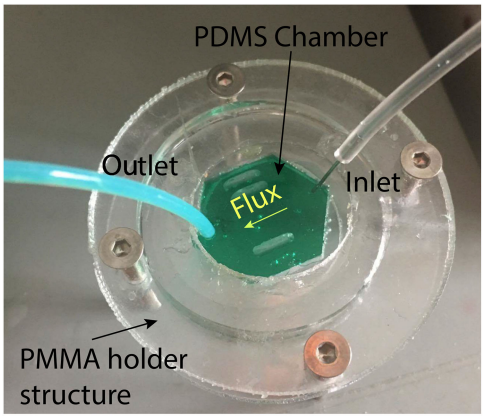

Fig. 6. The PDMS fluidic chamber with the PMMA holder.

2) Fluidic Fabrication and the Electrochemical Platform Integration: The fluidic chamber consists of two parts: (i) a top layer where three holes were punched to insert the three electrodes for the electrochemical detection and (ii) a bottom layer containing the mixing soft-walls. To fabricate the bottom layer chamber, a 3 mm *Poly(methyl methacrylate)* (PMMA) mold has been fabricated by designing the geometry in *Inkscape* software first and then printing with a *Full Spectrum laser retina engrave 3D*. The PDMS (1:10) part, mixing, de-bubbling, pouring and curing in 80° C oven has been done in the *Center of Microtechnology* at EPFL. A PMMA structure with four screws has been printed with the laser cutter to assemble the two parts of the chamber in a sandwich structure, as shown in Fig. 6.

The three-electrode electrochemical cell consists of a PGE as WE, a K0265 Ag/AgCl electrode from Ametek Scientific Instruments as RE and a Pt wire as CE. The PGE is made up of a composite material containing graphite, clay and a wax as binder in the percentage of 58%, 36% and 5%, respectively. The Staedtler Mars Lumograph Wood Pencil *3H* was adopted and purchased by Cult Pens (United Kingdom). The two extremities of the pencil have been peeled to obtain from one side the WE active area ($\sim$12.6 mm^2) and from the other side the electronic connection with the dedicated hardware.

3) Chemicals: 2,6-Diisopropylphenol (Propofol) was purchased from TCI chemical and dissolved in 0.1 M NaOH to prepare the stock solution of 5.4 mm. Subsequent dilutions of propofol stock solution were prepared in *Phosphate Buffer Saline* (PBS) (10 mm, pH:7.4) or in serum to obtain concentrations in the range [9.9–80.5] μM. The compounds *Paracetamol* (APAP), NaOH and heat inactivated human male serum were purchased from Sigma Aldrich (Switzerland). APAP stock solution 30 mm was prepared by dissolving 5 mg of APAP powder in 1 ml PBS (10 mm, pH:7.4). Subsequent dilutions of APAP stock solution were done in PBS or serum in the range [50–300] μM .

B. Validation of the System

Final aim of our validation procedure was to verify the performance of our system in detecting the two complementary anesthetic compounds, e.g., propofol and APAP, under flow conditions in human serum. Before reaching this goal, some preliminary test have been performed.

TABLE III
FLUX VELOCITIES EVALUATION

Pump Velocity (rpm)	Time to fill (s)	Velocity (μL/s)
48	5	10.4
47	5.8	8.9
46	6.4	8.1
45	6.7	7.7
44	7.3	7.1
43	7.5	6.9
42	9	5.7

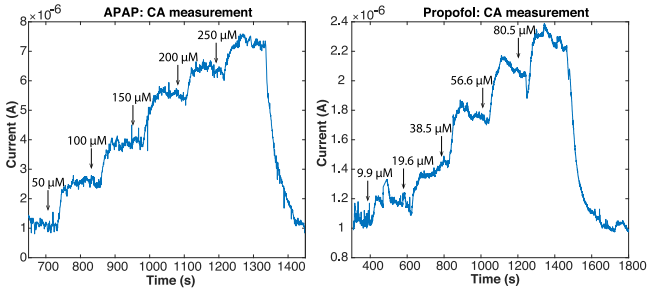

(a) (b)

Fig. 7. CA measurements for: (a) APAP and (b) propofol drugs.

1) Characterization of the Fluidic System: First important step was to find the correspondence between the internal velocities of the peristaltic pump (*Gilson Minipuls 3*) armed with a *Polyvinyl chloride* (PVC) tube (diameter = 0.38 mm, length = 460 mm and volume = 52 μL) and the effective fluid flux. Hereafter, in Table III, we report the results. A velocity of 46 rpm or 48 rpm was adopted for the measurements in flow conditions to test our system by simulating the fastest variability rate of the drug concentration possible with our setup.

Then we had to optimize the mixing effect and timing for the fluidic system. Accordingly to the Comsol simulation results for different chamber geometries, in Fig. 4, we designed a PDMS hexagonal chamber with internal walls able to create a better mixing in the proximity of the electrodes. The mixing parameters have been qualitatively evaluated first by various dye solutions (Fig. 6). After this empirical characterization, the required time for ensuring the homogeneous drug concentration around sensing site was also evaluated. To that aim CA measurements in PBS solution for both APAP and propofol drugs were carried out. For APAP a fixed potential of 0.9 V was applied to the electrochemical cell by keeping the pump at 46 *revolutions per minute* (rpm) velocity while for propofol a 1 V potential was applied with a pump velocity of 48 rpm. After every 3 minutes, the drug samples have replaced with another one having higher drug concentration. Fig. 7 reports the two CA measurements for APAP and propofol. From these graphs it is possible to deduce that the steady state was reached after around 50 s by the increase of the drug concentration.

Based on this, 50 s can be considered as the minimum waiting time to ensure that in the electrochemical chamber the drug concentration is the same as to the one in the input beaker. The following DPV sensor calibrations in flow conditions were

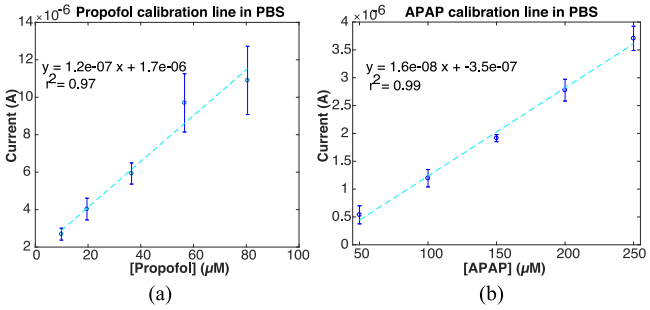

(a) (b)

Fig. 8. DPV calibration lines with standard error bars (n = 3) obtained under flow conditions in PBS electrolyte solution for: (a) proprofol and (b) paracetamol.

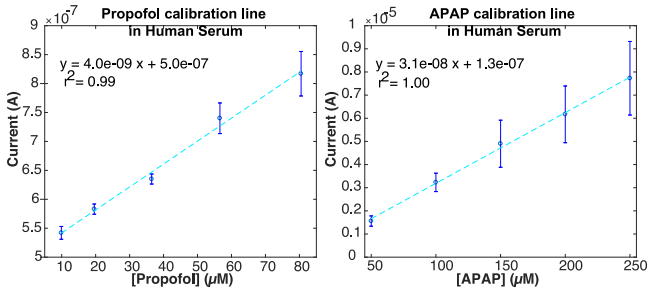

(a) (b)

Fig. 9. DPV calibration lines with standard error bars (n = 3) obtained under flow conditions in undiluted human serum for: (a) proprofol and (b) paracetamol.

performed by setting the pump at 48 rpm waiting 1 min 10 s between each measurement. To obtain better signal we stopped the flow while DPV procedure was running. Fig. 8 shows the 5-point calibration lines for the measurement of two drugs in PBS by DPV.

2) Human Serum Detection: In this subsection the simultaneous detection of paracetamol and propofol drugs has been achieved in undiluted human serum.

First, DPV calibrations in flow conditions (pump velocity 48 rpm), reported in Fig. 9, were carried out to characterize the system for propofol and APAP monitoring. Then two main crucial experiments were performed to assess the system performances:

- *Mixing test:* serum solution containing three different APAP concentrations (50–150–300 μM) was fluxed from lower to higher concentration (pump velocity 48 rpm) in the chamber and measured by the system every 1 min 30 s. Afterwards, while the APAP concentration was maintained at 300 μM, various propofol concentrations (20, 50 and 80 μM) were added to the solution and measurements were taken every 1 min 30 s for each concentration. Fig. 10 reports the obtained DPV curves from this experiment. It is evident from the figure that any peak is evident in the blank control measurement, obtained when fluxing undiluted human serum without any drug. After, only one peak at ~0.7 V (orange area) is visible when only APAP is present in the fluxed solution. The peak increases with the increase of the drug concentration. As soon as propofol drug is added in the solution (while APAP is kept constant) two other peaks at ~0.45 V and ~0.6 V (green areas) arise. The two peaks become higher when propofol concentration in the solution increases, while the APAP peak is not affected significantly. Therefore, we can conclude that these drugs does not interact with each other.
- *In-time monitoring test:* the chamber was filled with serum without any drug. Then, a serum solution containing 300 μM of APAP was fluxed (pump velocity 48 rpm) to the system. We performed one DPV measurement (30 s measurement time) every 10 s of fluxing of the APAP solution. After 12 min we have changed the fluxing solution with serum containing only 60 μM propofol. The same frequency of measurement was applied; a DPV every 10 s during 12 min. The exchange of the fluxing solutions was done in the 10 s of mixing in order to not interrupt the procedure. Fig. 11 reports the measured peak currents over time, which can be converted in drug concentration values

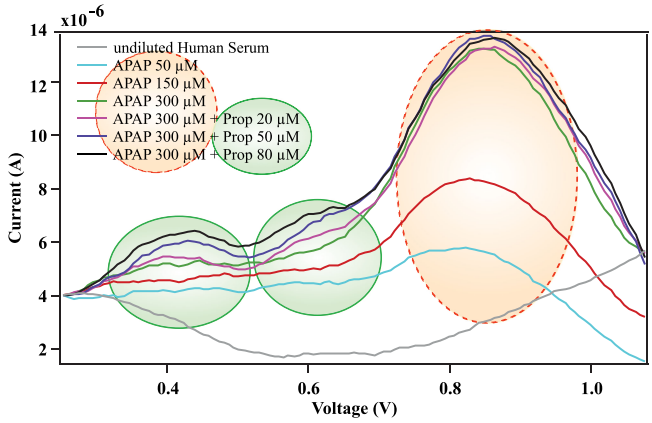

Fig. 10. *Mixing test*: DPV measurements in undiluted human serum fluxing (pump set at 48 r/min) a solution containing before three increasing concentrations of APAP (50–150–300 μM) and then three solutions with fixed APAP concentration (300 μM) and three increasing concentrations of propofol (20–50–80 μM). Blank measurement with no drug in fluxing serum solution is reported as control.

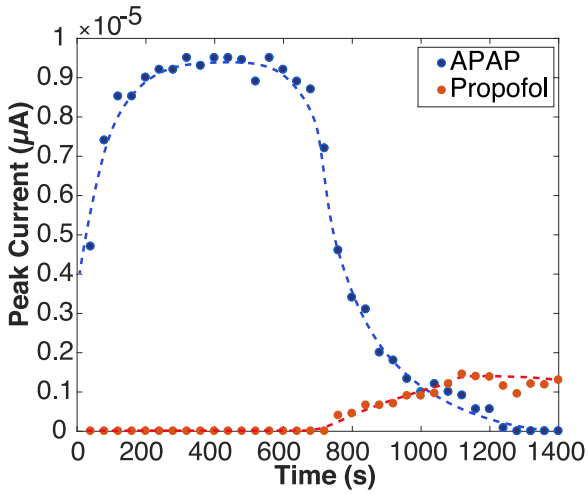

Fig. 11. *In-time monitoring test*: The concentration trends of APAP (300 μM) and propofol (60 μM) is monitored over time in undiluted human serum under fluxing conditions (pump set at 48 r/min).

according to the linear calibration equation expressed in Fig. 9. Therefore, to convert the current value in a concentration it is just needed to substitute the x parameter in the corresponding equation and the corresponding concentration is provided by the y estimation. To the aim of our analysis, we have preferred to keep the data in current values to be able to visualize the two trends of APAP and propofol on the same plot.

The results of human serum detection, mixing test and in-time monitoring test show that with our system, we are capable of in-time monitoring the change of concentration of two drugs, e.g., APAP and propofol, in undiluted human serum due to sample flux over a period of time.

IV. Conclusions

To reduce POPI effects in anesthesia infusion, paracetamol analgesic is often also administered in combination. In order to personalize and optimize the effects of these difficult-to-dose drugs, TDM on-line systems able to measure the drug concentrations in patient's plasma are highly required.

In this work, a novel IoT drug monitoring system with electrochemical approach for the on-line continuous and simultaneous detection of propofol and paracetamol has been shown. The design of each block of the system has been described from a system level: (i) the custom-built RPi-based circuit to control and read out the signal from (ii) the electrochemical cell, which is integrated in (iii) a fluidic device that flux the target solution in the chamber where the electrodes are immersed. The presented IoT solution is based on a dedicated Android application for the anesthesiologist's tablet or smart-phone to guarantee a rapid visualization of the patients' measured parameters. Through the application, the medical doctor can be alerted in case of out-of-safe-range parameter from a patient and can share and store the data on cloud to require teleconsulting.

The system was firstly characterized in PBS to evaluate the flux velocity and the mixing properties. Afterwards, it was proved that it efficiently works for the simultaneous detection of propofol and paracetamol in undiluted human serum. We have thus demonstrated, for the first time, the successful detection of the concentration of the two drugs over 24 min. The system also provides more than one channel and has potential to be used for multiplexed drug monitoring in the future.

Two further future improvements of the system would be addressed. First, knowing the electrical response of the sensing unit, it would worth to optimize the hardware design by using commercially available *Systems-on-a-Chip* (SoC)s to offer an even more portable solution with optimized dimensions. Second, we would like to include a feedback control algorithm, such as *Proportional-Integral-Derivative* (PID), to close the feedback loop with the TCI pump delivery system.

References

[1] G. Kotsovolis and G. Komninos, "Awareness during anesthesia: How sure can we be that the patient is sleeping indeed?," *Hippokratia*, vol. 13, no. 2, pp. 83–89, 2009.

[2] E. N. Brown, R. Lydic, and N. D. Schiff, "General anesthesia, sleep, and coma," *New England J. Med.*, vol. 363, no. 27, pp. 2638–2650, 2010.

[3] C. S. Nunes, D. A. Ferreira, L. Antunes, and P. Amorim, "Clinical variables related to propofol effect-site concentrations at recovery of consciousness after neurosurgical procedures," *J. Neurosurg. Anesthesiol.*, vol. 17, no. 2, pp. 110–114, 2005.

[4] B. Larsen, A. Seitz, and R. Larsen, "Recovery of cognitive function after remifentanil-propofol anesthesia: A comparison with desflurane and sevoflurane anesthesia," *Anesthesia Analgesia*, vol. 90, no. 1, pp. 168–174, 2000.

[5] V. Chidambaran, A. Costandi, and A. D'Mello, "Propofol: A review of its role in pediatric anesthesia and sedation," *CNS Drugs*, vol. 29, no. 7, pp. 543–563, 2015.

[6] H. Borazan, T. B. Erdem, M. Kececioglu, and S. Otelcioglu, "Prevention of pain on injection of propofol: A comparison of lidocaine with different doses of paracetamol," *Eur. J. Anaesthesiol.*, vol. 27, no. 3, pp. 253–257, 2010.

[7] K. A. Desousa, "Pain on propofol injection: Causes and remedies," *Indian J. Pharmacol.*, vol. 48, no. 6, p. 617–623, 2016.

[8] L. F. Prescott, "Paracetamol: Past, present, and future." *Amer. J. Therapeutics*, vol. 7, no. 2, pp. 143–147, 2000.

[9] Z. Al-Rifai and D. Mulvey, "Principles of total intravenous anaesthesia: Practical aspects of using total intravenous anaesthesia," *BJA Educ.*, vol. 16, no. 8, pp. 276–280, 2016.

[10] S. L. Shafer and K. M. Gregg, "Algorithms to rapidly achieve and maintain stable drug concentrations at the site of drug effect with a computer-controlled infusion pump," *J. Pharmacokinet. Biopharm.*, vol. 20, no. 2, pp. 147–169, 1992.

[11] D. J. Eleveld, J. H. Proost, L. I. Cortínez, A. R. Absalom, and M. M. Struys, "A general purpose pharmacokinetic model for propofol," *Anesthesia Analgesia*, vol. 118, no. 6, pp. 1221–1237, 2014.

[12] L. O. Boréus, "The role of therapeutic drug monitoring in children," *Clin. Pharmacokinet.*, vol. 17, no. 1, pp. 4–12, 1989.

[13] S. Layne, G. Mayer-Kress, and J. Holzfuss, "Problems associated with dimensional analysis of electroencephalogram data," in *Proc. Dimensions Entropies Chaotic Syst*. 1986, pp. 246–256.

[14] I. Kissin, "Depth of anesthesia and bispectral index monitoring," *Anesthesia Analgesia*, vol. 90, no. 5, pp. 1114–1117, 2000.

[15] G. Schneider, E. F. Kochs, B. Horn, M. Kreuzer, and M. Ningler, "Narcotrend does not adequately detect the transition between awareness and unconsciousness in surgical patients," *Anesthesiology: J. Amer. Soc. Anesthesiol.*, vol. 101, no. 5, pp. 1105–1111, 2004.

[16] J. Wang, "Electrochemical biosensors: Towards point-of-care cancer diagnostics," *Biosensors Bioelectron.*, vol. 21, no. 10, pp. 1887–1892, 2006.

[17] S. Carrara, "Bio/CMOS interfaces in constant bias." Bio/CMOS Interfaces and Co-Design, Springer New York, NY, pp. 185–205, 2013.

[18] B. Xu, L. Da Xu, H. Cai, C. Xie, J. Hu, and F. Bu, "Ubiquitous data accessing method in IoT-based information system for emergency medical services," *IEEE Trans. Ind. Inf.*, vol. 10, no. 2, pp. 1578–1586, May 2014.

[19] A. Santos, J. Macedo, A. Costa, and M. J. Nicolau, "Internet of things and smart objects for m-health monitoring and control," *Procedia Technol.*, vol. 16, pp. 1351–1360, 2014.

[20] M. H. Myers, Y. Li, F. Kivlehan, E. Lindner, and E. Chaum, "A feedback control approach to organic drug infusions using electrochemical measurement," *IEEE Trans. Biomed. Eng.*, vol. 63, no. 3, pp. 506–511, Mar. 2016.

[21] S. S. Ghoreishizadeh, I. Taurino, S. Carrara, and G. De Micheli, "A current-mode potentiostat for multi-target detection tested with different lactate biosensors," in *Proc. IEEE Biomed. Circuits Syst. Conf.*, 2012, pp. 128–131.

[22] J. Yarbrough, R. Harvey, and S. Cox, "Determination of propofol using high performance liquid chromatography in whole blood with fluorescence detection," *J. Chromatographic Sci.*, vol. 50, no. 3, pp. 162–166, 2012.

[23] F. Vaiano, G. Serpelloni, M. Focardi, A. Fioravanti, F. Mari, and E. Bertol, "Lc–ms/ms and gc–ms methods in propofol detection: Evaluation of the two analytical procedures," *Forensic Sci. Int.*, vol. 256, pp. 1–6, 2015.

[24] F. Kivlehan, E. Chaum, and E. Lindner, "Propofol detection and quantification in human blood: The promise of feedback controlled, closed-loop anesthesia," *Analyst*, vol. 140, no. 1, pp. 98–106, 2015.

[25] J. Langmaier, F. Garay, F. Kivlehan, E. Chaum, and E. Lindner, "Electrochemical quantification of 2, 6-diisopropylphenol (propofol)," *Analytica Chimica Acta*, vol. 704, no. 1–2, pp. 63–67, 2011.

[26] C.-C. Hong, C.-C. Lin, C.-L. Hong, Z.-X. Lin, M.-H. Chung, and P.-W. Hsieh, "Handheld analyzer with on-chip molecularly-imprinted biosensors for electrical detection of propofol in plasma samples," *Biosensors Bioelectron.*, vol. 86, pp. 623–629, 2016.

[27] F. Stradolini, A. Tuoheti, P. M. Ros, D. Demarchi, and S. Carrara, "Raspberry pi based system for portable and simultaneous monitoring of anesthetics and therapeutic compounds," in *Proc. New Generation CAS*, 2017, pp. 101–104.
[28] E. Ghodsevali *et al.*, "Miniaturized fdda and cmos based potentiostat for bio-applications," *Sensors*, vol. 17, no. 4, 2017, Art. no. 810.
[29] P. Bezuidenhout, K. Land, and T. Joubert, "A low-power CMOS operational amplifier ic for a heterogeneous paper-based potentiostat," in *Proc. Fourth Conf. Sensors, MEMS Electro-Optic Syst*, 2017, pp. 100360P.
[30] S. Ghoreishizadeh, E. G. Kilinc, C. Baj-Rossi, C. Dehollain, S. Carrara, and G. De Micheli, "An implantable bio-micro-system for drug monitoring," in *Proc. IEEE Biomed. Circuits Syst. Conf.*, 2013, pp. 218–221.
[31] F. Basilotta *et al.*, "Wireless monitoring in intensive care units by a 3d-printed system with embedded electronic," in *Proc. IEEE Biomed. Circuits Syst. Conf.*, 2015, pp. 1–4.
[32] M. Integrated, *SOT23, Low-Noise, Low-Distortion, Wide-Band, Rail-to-Rail Op Amps*, 2018. [Online]. Available: https://www.maximintegrated.com/en/products/analog/amplifiers/MAX4475.html
[33] E. Hub, *Butterworth Filter*, 2015. [Online]. Available: https://www.electronicshub.org/butterworth-filter/
[34] H. L. Fernandez-Canque, *Analog Electronics Applications: Fundamentals of Design and Analysis*. CRC Press, 2016.
[35] X. Yang, J. Kirsch, J. Fergus, and A. Simonian, "Modeling analysis of electrode fouling during electrolysis of phenolic compounds," *Electrochimica Acta*, vol. 94, pp. 259–268, 2013.
[36] F. Stradolini, T. Kilic, A. Di Consiglio, M. Ozsoz, G. De Micheli, and S. Carrara, "Long-term monitoring of propofol and fouling effect on pencil graphite electrodes," *Electroanalysis*, no. 30, pp. 1363–1369, 2018.
[37] F. Stradolini, T. Kilic, I. Taurino, G. De Micheli, and S. Carrara, "Cleaning strategy for carbon-based electrodes: Long-term propofol monitoring in human serum," *Sensors Actuators B: Chem.*, 2018, vol. 269, no. 15, pp. 304–313, 2018.
[38] S. L. Ntella, F. Stradolini, A. Tuoheti, D. Demarchi, A. A. Hatzopoulos, and S. Carrara, "Architecture and procedures for ph and temperature monitoring in medical applications," in *Proc. IEEE Sensors*, 2017, pp. 1–3.
[39] J. Janata and M. Josowicz, "Peer reviewed: A fresh look at some old principles: The kelvin probe and the nernst equation," *Analytical Chemistry*, vol. 69, no. 9, pp. 293A–296A, 1997.
[40] "*What Are the Navier-Stokes Equations?*," Multiphysics Cyclopedia Comsol, 2018. [Online]. Available: https://www.comsol.com/multiphysics/navier-stokes-equations
[41] L. T. Sniegoski and J. R. Moody, "Determination of serum and blood densities," *Analytical Chemistry*, vol. 51, no. 9, pp. 1577–1578, 1979.
[42] M. L. Eginton, "Evaluation of the effectiveness of a commercial cooling collar in reducing body temperature during heat stress: theoretical modeling of body temperature distribution," Ph.D. dissertation, Univ. Maryland, MD, 2007.
[43] F. Stradolini, N. Tamburrano, T. Modoux, A. Tuoheti, D. Demarchi, and S. Carrara, "Iot for telemedicine practices enabled by an android application with cloud system integration," in *Proc. IEEE Int. Symp. Circuits Syst.*, 2018, doi: 10.1109/ISCAS.2018.8351871

Authors' photographs and biographies not available at the time of publication.